Pure appl. geophys. 159 (2002) 2673–2698
0033–4553/02/122673–26 $ 1.50 + 0.20/0

Pure and Applied Geophysics

Determination of S-wave Site Response in Anchorage, Alaska in the 1–9 Hz Frequency Band

Sankar Kumar Nath,[1] Nirendra N. Biswas,[2] Marijan Dravinski,[3] and Apostolos S. Papageorgiou[4]

Abstract—Site response was estimated at 19 sites in the Anchorage basin in south-central Alaska, using 15 local earthquakes recorded with good signal-to-noise ratio by a temporary weak motion network. The receiver-function-type horizontal-to-vertical spectral ratios (HVSR) were computed at 1–9 Hz frequency band and the resulting HVSR contour maps at 1, 5 and 9 Hz are presented here. The spatial site response distribution shows considerable variation from the foothills of the Chugach Mountains in the east to the western part of Anchorage. The site response increases by a factor of 3 and 3.5 at 1 and 5 Hz, respectively, from the area of older glacial deposits in the eastern part of the city to the area occupied by the Bootlegger Cove formation, particularly in the section adjoining Knik Arm. At 9 Hz, the variation of HVSR from the east to the west is smaller, approximately by a factor of 2. Moreover, the trend of the HVSR variation at 1 and 5 Hz shows good correlation with that of the soil class obtained from surface measurements of *S*-wave velocity in the 0–30 m depth range and available results on ground failure susceptibility of Anchorage.

Key words: Ground failure susceptibility, horizontal-to-vertical spectral ratios, National Earthquake Hazard Reduction Program, site response, soil class.

1. Introduction

The level of seismic risk in Anchorage as compared to other metropolitan areas in the United States is high (Whitman, 1989). The peak ground acceleration anticipated in Anchorage and cities in California is several times greater than that in the central and eastern United States, for all exposure times. Many sites in and around Anchorage, particularly along the coast of Knik and Turnagain Arms

[1] Department of Geology and Geophysics, Indian Institute of Technology, Kharagpur 721 302, West Bengal, India. E-mail: nath@gg.iitkgp.ernet.in, Formerly Visiting Scientist, Geophysical Institute, University of Alaska Fairbanks, U.S.A.

[2] Geophysical Institute, University of Alaska Fairbanks, AK99775-7320, U.S.A. E-mail: niren@giseis.alaska.edu

[3] Department of Mechanical Engineering, University of Southern California, 3650 McClintock Ave, Room 430, Los Angeles, CA 90089-1453, U.S.A. E-mail: mdravins@mizar.usc.edu

[4] State University of New York at Buffalo, Department of Civil, Structural and Environmental Engineering, Ketter Hall 222, Buffalo, NY 14260-4300, U.S.A. E-mail: papaga@eng.buffalo.edu

(Fig. 1) experienced extensive ground failure during the 1964 Prince William Sound earthquake ($M_w = 9.2$) in Alaska. A large section of the city lies in a sedimentary basin with the bedrocks exposed in the Chugach Mountains, which lie on the eastern side of the city. The sedimentary section immediately overlying the bedrock is the Kenai formation of Tertiary age constituting the major unit of Cenozoic sequence. It consists of several hundred meters of non-marine sediments, principally sandstone, siltstone and claystone containing localized coal seams. Except for a few small exposures, it is covered by several hundred meters of Quaternary sediments.

Quaternary deposition in the area includes extensive glacial deposits from at least five glacial advances into the lowlands from the surrounding ranges. Glacial

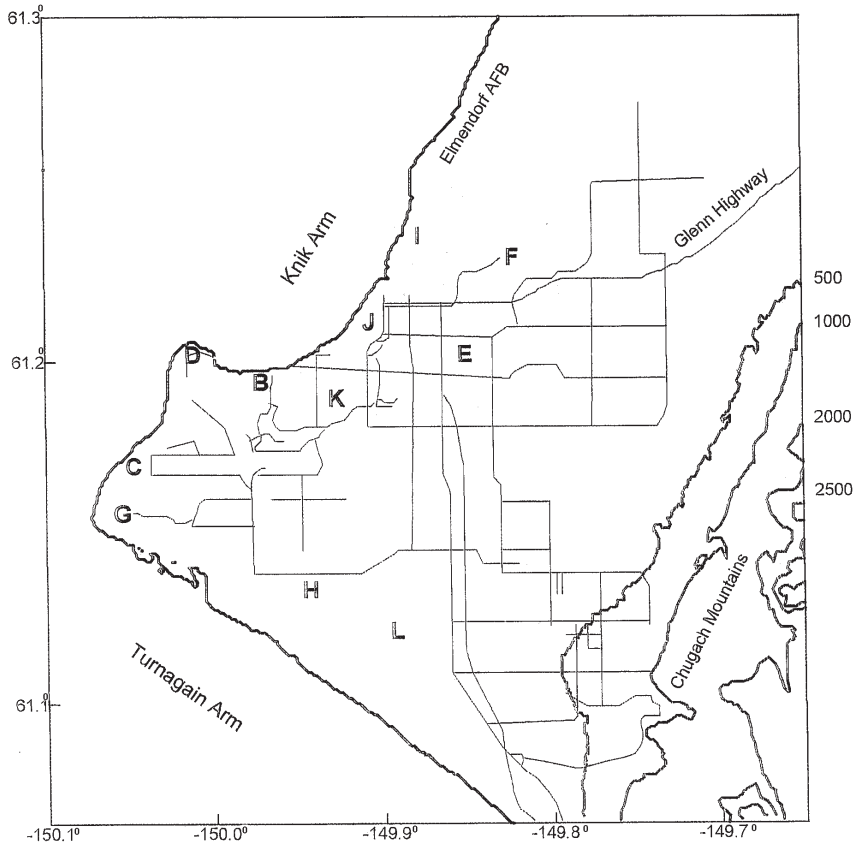

Figure 1

Map of metropolitan area of Anchorage. Knik and Turnagain Arms are part of Cook Inlet, which connects to the Gulf of Alaska in the south. The thick contour lines of Chugach Mountains represent elevation in feet and thin lines are major roads in Anchorage. The letters mark the following places, some of which have been referred in the text: B — Earthquake Park; C — International Airport; D — Pt. Woronzof; E — Merrill Field; F — Mt. View; G — Kincaid Park; H — Campbell Lake; I — Govt. Hill; J — Westchester Lagoon; K — Woodland Park; L — KHAR Tower.

sedimentation resulted in irregular heterogeneous deposits of mixed clay, silt, sand and gravel, ranging from moderately well stratified to unstratified; the more poorly stratified are glacial moraine deposits from clay to boulder. Large areas of morainal deposits extend from the southeast side of Knik Arm to the lower Chugach Range front.

An important component of the Quaternary deposition is the lacustrine marine deposit termed the Bootlegger Cove formation that underlies the lowland area at shallow depth in a north-south oriented zone several miles wide (Fig. 2, YEHLE *et al.*, 1986). This zone includes most of metropolitan Anchorage, and it is susceptible to liquefaction as exhibited during the 1964 event mentioned above. The surficial

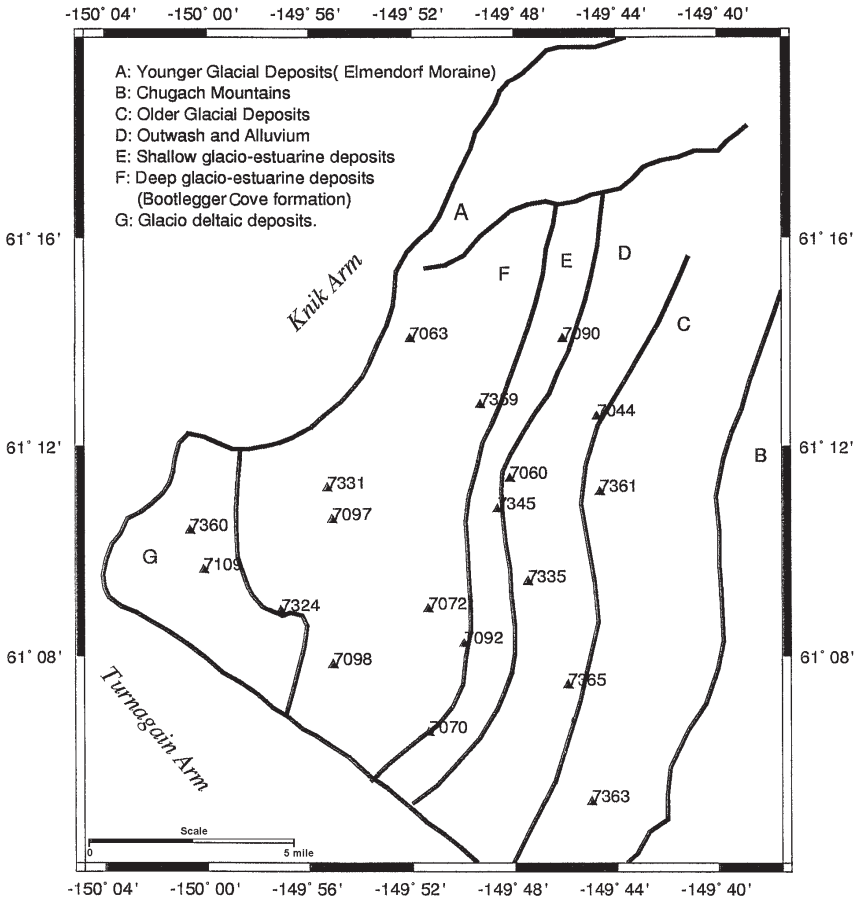

Figure 2
Locations of IRIS-PASSCAL (Incorporated Research Institute for Seismology-Program for the Array Seismic Studies of the Continental Lithosphere) stations shown by 4-digit numbers (Table 1) on a surficial geological map of Anchorage.

deposits overlying Bootlegger Cove formation in Anchorage are mostly fluvial and glaciofluvial sand and gravel with a thin cover of wind-deposited silt and sand.

The first-order features of the seismotectonic setting of the greater Anchorage area consists of the underthrusting of the Pacific plate beneath the North American plate (RATCHKOVSKY *et al.*, 1997). The underthrusting occurs at a rate of about 5.59 cm/yr in the northwest direction in the Gulf of Alaska as shown in Figure 3(a). This phenomenon, besides giving rise to active volcanism, imparts stresses in the lithosphere which causes earthquakes along faults in the overriding North American plate, along the interface between the North American and Pacific plates (megathrust), and within the underthrust Pacific plate (Wadati-Benioff-Zone, WBZ hereinafter).

Several faults (Fig. 3b) lie in the overriding North American plate; of these, two faults, Lake Clark-Castle Mountain and Border Ranges, in addition to the megathrust and WBZ, are potential sources of seismic hazard to Anchorage. Lake Clark-Castle Mountain fault lies about 40 km from Anchorage, trending northeast-southwest. Both surface and subsurface (trenching) mapping revealed late Holocene north-dipping reverse movement with a dextral component of lateral motion; focal mechanism studies indicated predominantly dextral slip along this fault (LAHR *et al.*, 1986). By correlating a sequence of well-controlled locations of aftershocks of a magnitude 5.7 earthquake (1984) with the mapped trace of the Lake Clark-Castle Mt. Fault, it was shown by the above authors that the major part of this fault lying due north of Anchorage is currently active.

The Border Ranges fault in Anchorage and the neighboring area is largely covered by surficial deposits; its location, therefore, is not well defined. However, it has been inferred by UPDIKE and ULERY (1983) as to follow closely the base of the Chugach Mountains directly east of Anchorage (Fig. 1). To date, no well-defined spatial association between the seismicity and mapped trace of Border Ranges fault has been established.

Of the two faults mentioned earlier, the favorable geological conditions along the Lake Clark-Castle Mt. Fault allowed its more thorough investigation, leading to the identification by WOODWARD CLYDE CONSULTANTS (1982) of a "characteristic earthquake" with a magnitude M 7.5 near Anchorage. The Border Ranges fault potentially generates around magnitude (M) 7.0 earthquakes by the regional tectonic forces. Using the earthquake catalog, WOODWARD CLYDE CONSULTANTS (1982) estimated a maximum megathrust earthquake of moment magnitude (M_w) 9.5. Similarly, they estimated the maximum WBZ earthquake of surface wave magnitude (M_s) 7.5. On the basis of an average displacement of 10 m observed during the 1964 (M_w = 9.2) earthquake and convergence rate of 5 to 6 cm/yr, one obtains a recurrence interval of 160 to 200 years for a very destructive megathrust earthquake for the south-central coastal area of Alaska.

Following the large 1964 earthquake, seismic hazards in Anchorage have become a major concern to the inhabitants of the city. Lately, this has become a pervasive

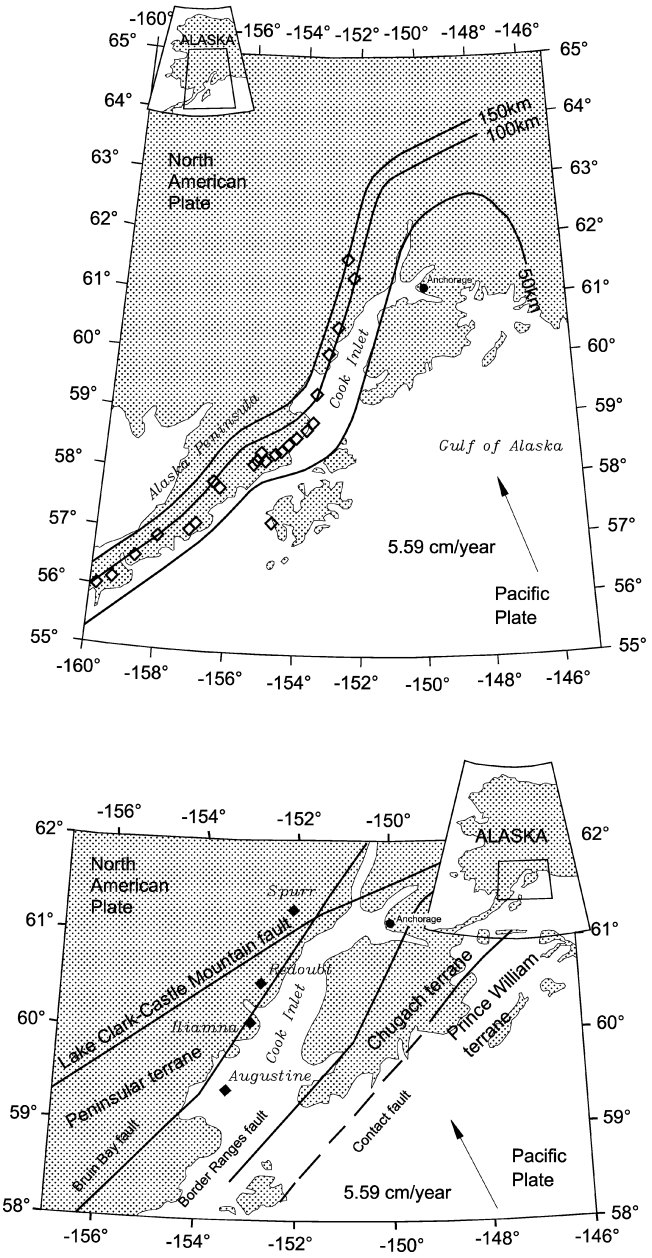

Figure 3

(a) Solid lines represent depth contour of the upper surface of the subducted Pacific Lithospheric plate in Southcentral Alaska. The arrow and the associated figure show the direction and rate, respectively, of the convergence of the Pacific and North American plates in the Gulf of Alaska. The diamonds are locations of active volcanoes in the Cook Inlet area and Alaska Peninsula. (b) Solid and broken lines, respectively, show the traces of mapped and inferred faults in the same area as in Figure 3(a).

issue, as Anchorage and its neighborhood continue to grow and become more complex. Though somewhat slowed recently, the area population grew at an annual rate of about 18% during the 1970s and most of the 1980s. This gave rise to high-rise buildings, expanded lifeline networks, transportation systems, etc., which significantly enhanced the potential of seismic risk to life and property, compared to the 1960s, for the greater Anchorage area. On the other hand, due to a lack of site-specific information on strong ground motion, city planners, architects, and engineers are unable to recommend adequate mitigation measures against potential seismic hazards for construction practices for the largest population center of the state of Alaska.

In order to address the above problems, we implemented a seismic microzonation project by deploying a temporary three-component, 19 portable IRIS-PASSCAL station network in Anchorage in the summer of 1994. The determination of site response under the strong influence of near-surface geological conditions at predominant frequencies during an earthquake constitutes an important part of the project.

There are many factors that influence the way a site will respond to earthquake ground motion (AKI, 1988; AKI and IRIKURA, 1991; BARD, 1994). These include: i) The source location, which influences the angle, azimuth, and type of incident waves; ii) the prevalence of energy focussed or scattered from lateral heterogeneities, such as surface waves generated at the edge of a basin which propagate as energy trapped within the sediments; and iii) the degree to which sediments behave nonlinearly, which causes the response to depend on the level of input motion. The greatest challenge in estimating site response from earthquake data is removing the source and path effects. The most common procedure, introduced by BORCHERDT (1970), is to divide the spectrum observed at the site in question by that observed at a nearby reference site (preferably on competent bedrock). If the two sites have similar source and path effects, and if the reference site has a negligible site response, then the resulting spectral ratio constitutes an estimate of site amplification. ANDREWS (1986) recast the method of spectral ratios into a generalized inverse problem by solving the data of multiple recorded events for all source/path effects and site effects simultaneously. These techniques for estimating site amplification depend on the availability of an adequate reference site with negligible site effect. Since such a site may not always be available, as in the present case, it is desirable to develop alternative methods that do not depend on a reference site. The first alternative method employs a generalized inversion scheme introduced by BOATWRIGHT *et al.* (1991), where shear-wave spectra are represented with a parameterized source and path-effect model and a frequency-dependent site response term for each site. The second non-reference-site-dependent technique involves dividing the horizontal component shear-wave spectra at each site by the vertical component spectrum observed simultaneously at that site (LERMO *et al.*, 1993). This procedure, which is analogous to the so-called receiver-function technique applied to studies of the upper mantle and crust from teleseismic records (e.g., LANGSTON, 1979; AMMON and

ZANDT, 1993), assumes that the local site conditions are relatively transparent to the motion that appears on the vertical component.

The present site response study is based on weak motion data. In the following we report the results obtained from the non-reference horizontal-to-vertical component spectral ratio site response analysis of the data recorded by the IRIS-PASSCAL (I-P) network in Anchorage.

2. Data Source

The IRIS-PASSCAL (I-P) network was operated in Anchorage for one and one-half months. Each station consisted of a 4.5 Hz three-component seismometer (Mark Product L-28) connected to a 440 MB Reftek recorder with a GPS receiver; data were recorded at 100 Hz sampling rate. At 1 Hz, the recording gain dropped by about 30 dB from the peak gain level. However, as shown later, the data for a number of local earthquakes could be recorded with good signal-to-noise ratio from 1 to 9 Hz. Of course, we had to correct the amplitude of the signal to take into account the sensitivity of the sensors used in recording the events.

The I-P network stations were located on different geological formations (Fig. 2) with the exception of zone A (younger glacial deposits) and B (Chugach Mountains). This is because the area in zone A is outside the scope of the present study and in B we could provide no seismographic coverage due to logistic difficulties. Conversely, the area in zone B represents rock site. Thus, this study lacked seismic data representative of a rock site. The details of the station locations are listed in Table 1.

Of many dozens of local earthquakes recorded, the present analysis is based on 15 events which were recorded with good signal-to-noise ratio. The locations of the epicenters (solid circles) of these events are shown in Figure 4 and their details are given in Table 2. The magnitudes of the events selected range from 3.0 to 4.7. Table 3 shows the stations which recorded each selected earthquake used in this study.

3. Data processing

Assume j events have been recorded by a network of i stations (each event may not be recorded by all i stations). Then the amplitude spectrum of the j-th event recorded at the i-th station, for the k-th frequency, say $O_{ij}(f_k)$ can be written in the frequency domain as a product of a source term $SO_j(f_k)$, a path term $P_{ij}(f_k)$, and site-effect term $S_i(f_k)$:

$$O_{ij}(f_k) = SO_j(f_k) \cdot P_{ij}(f_k) \cdot S_i(f_k) \quad . \tag{1}$$

Taking the natural logarithm, (1) becomes,

Table 1

Seismic station locations used in the site response study

No.	Station no.	Station site	Longitude (W)	Latitude (N)	Elevation (m)
1	7090	Elmendorf Air Force Base-USGS	149°46.10′	61°14.07′	61.3
2	7063	Elmendorf Air Force Base-GI	149°52.09′	61°14.07′	44
3	7359	Fire Station No. 3	149°49.35′	61°12.79′	35
4	7044	Fire Station No. 6	149°44.74′	61°12.57′	78
5	7361	Scenic Park High School	149°44.64′	61°11.13′	96
6	7060	Alaska Pacific University	149°48.20′	61°11.38′	60
7	7345	Municipality of Anchorage Dept. of P.W.	149°48.69′	61°10.80′	60
8	7331	Fire Station No. 5	149°55.30′	61°11.20′	25
9	7360	Weather Station (NOAA)	150°00.67′	61°10.39′	30
10	7324	Fire Station No. 7	149°57.11′	61°08.86′	30
11	7072	Fire Station Headquarters	149°51.39′	61°08.89′	35
12	7335	Bureau of Land Management	149°47.49′	61°09.42′	70
13	7098	South Anchorage Baptist Church	149°55.08′	61°07.83′	15
14	7070	Fire Station No. 9	149°51.37′	61°06.52′	45
15	7365	Fire Station No. 8	149°45.92′	61°07.44′	140
16	7363	Fire Station No. 10	149°45.00′	61°05.20′	280
17	7109	Federal Common Commission	150°00.13′	61°09.64′	35
18	7097	School District Warehouse	149°55.11′	61°10.60′	27
19	7092	Radio Station	149°49.99′	61°08.23′	65

$$\ln O_{ij}(f_k) = \ln SO_j(f_k) + \ln P_{ij}(f_k) + \ln S_i(f_k) \ . \tag{2}$$

This linear expression often forms the basis of attempts to separate the source, path, and site-effects (FIELD and JACOB, 1995; DIMITRIU *et al.*, 1998).

LERMO *et al.* (1993) presented evidence that site response can be estimated by taking horizontal-to-vertical component ratios of the shear-wave spectra. This technique was originally introduced by NAKAMURA (1989) to analyze ambient seismic noise recordings. However, LERMO *et al.* (1993) applied the method to earthquake data obtained at various sediment sites in Mexico and found that the frequency and amplitude of the fundamental resonant peak could be identified. LANGSTON (1979) applied a method of determining the velocity structure of the crust and upper mantle from teleseismically recorded *P* waves. The vertical component is

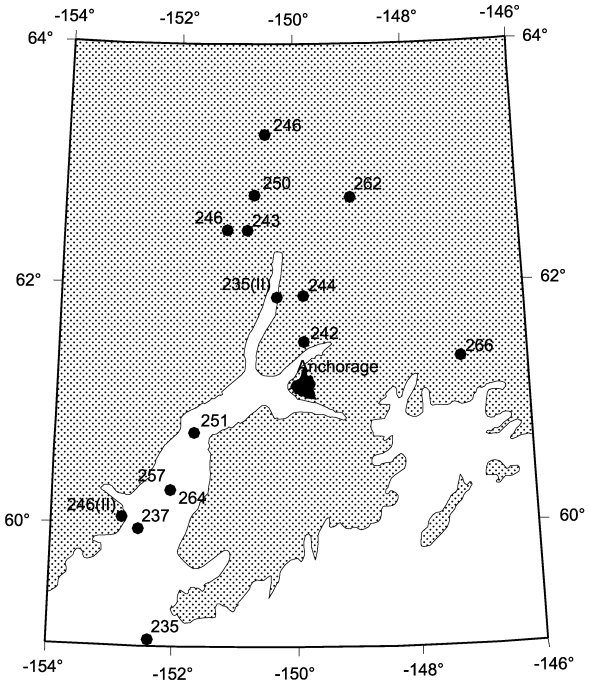

Figure 4
Locations of the epicenters of earthquakes used in the present study shown with respect to that of Anchorage.

assumed to be relatively uninfluenced by the local structure, whereas the radial component contains *P*- and *S*-wave conversions from structural discontinuities below the site. Therefore, by deconvolving the vertical component from the radial, an estimate of the impulse response function, or receiver function, is obtained below the site. Many receiver function studies have since been applied to study the earth's crust and mantle (e.g., OWENS *et al.*, 1984; OWENS and CROSSEN, 1988). By analogy, one might expect the method to apply to smaller-scale features of sedimentary layers. Here, the vertical component of shear waves could be composed primarily of *S*- to *P*-wave conversions, as has been observed in borehole studies (TAKAHASHI *et al.*, 1992), which may be relatively uninfluenced by the sediments. If this were true, then an estimate of the site response could be obtained by deconvolving, or dividing in the frequency domain, the vertical component from the horizontal component. Since in Anchorage we lacked a rock site data coverage due to a logistic problem, we considered the receiver function estimate 'HVSR' as the representative of the site response.

At first we bandpass-filtered (Butterworth) each seismogram within 0.5 to 16 Hz frequency range for each event. For example, Figures 5a(i), 5b(i) and 5c(i) represent the unfiltered three-component raw data recorded at station 7360 (Fig. 2) for the

Table 2

Location of 15 earthquakes used in the present site response study

No.	Date yr:mo:dy	Julian day	Origin time hr:min:sec	Lat. (°N)	Long. (°W)	Depth (km)	Mag. (ML)
1	94:08:23	235	14:33:52.83	59.06	152.40	87.72	4.7
2	94:08:23	235(II)	15:09:44.37	61.90	150.31	00.00(?)	3.0
3	94:08:25	237	02:56:25.14	59.98	152.59	81.76	4.3
4	94:08:30	242	05:56:03.99	61.53	149.85	44.15	3.4
5	94:08:31	243	19:26:08.38	62.81	150.81	90.28	3.0
6	94:08:01	244	21:38:55.34	61.91	149.82	06.39	3.1
7	94:09:03	246	06:56:14.75	62.46	151.14	89.74	3.1
8	94:08:03	246(II)	22:59:35.61	60.07	152.84	89.73	3.0
9	94:09:05	248	17:23:56.55	63.25	150.52	130.38	3.2
10	94:09:07	250	18:40:52.63	62.75	150.69	102.84	4.1
11	94:09:08	251	23:06:06.20	60.78	151.68	70.66	3.4
12	94:09:19	262	12:41:28.37	62.73	149.00	63.06	3.1
13	94:09:21	264	10:18:16.38	60.29	152.05	64.90	3.5
14	94:09:23	266	16:16:56.10	61.40	147.13	13.45	3.7
15	94:09:24	267	03:32:33.37	60.31	152.05	64.90	3.1

Table 3

Earthquake recording history by the IRIS-PASSCAL network in Anchorage, Alaska. The asterisks indicate that the event was recorded at that station site

Event no.	Julian day	7060	7063	7070	7072	7090	7092	7098	7109	7324	7331	7335	7345	7359	7360	7361	7363	7365
1	235	*	*	*	*			*	*	*		*	*	*	*		*	*
2	235(II)	*		*	*			*	*	*	*	*	*	*	*		*	
3	237	*	*	*	*	*		*	*	*	*	*	*	*	*		*	
4	242		*				*			*		*		*				
5	243		*				*			*			*	*	*			
6	244		*				*			*					*			
7	246			*				*					*	*	*	*		
8	246(II)			*				*		*			*	*	*	*		
9	248		*					*	*				*		*	*		
10	250	*	*				*	*	*			*	*	*	*	*		
11	251	*	*				*	*	*			*		*	*			
12	262	*	*	*			*	*		*			*	*	*	*	*	
13	264	*		*				*		*			*	*	*	*	*	
14	266	*	*	*			*	*	*	*		*	*	*	*	*	*	
15	267	*	*							*		*			*		*	

event 237 (Table 2). The filtered (0.5 –16 Hz) data are shown in Figures 5a(ii), 5b(ii) and 5c(ii), respectively. These data were scanned to select the *S*-wave window of the signal. The window width varied from 30 to 50 sec. Next we obtained the smoothed amplitude spectrum ($A_{ij}(f)$) using the five-point average of the *S*-wave windowed data (Figs. 5a(iii), 5b(iii) and 5c(iii)). Similarly, we obtained the amplitude spectrum ($B_{ij}(f)$) of the pre-event (background) section of the seismogram (Figs. 5a(iv), 5b(iv) and 5c(iv)). The amplitude spectra within 0.5–16 Hz for the *S*-wave and background windows are further displayed in Figures 6a, b and c in log-log scale for clarity. We advocate estimating the observational uncertainty directly from the data after eliminating all data for which the observed signal-to-ambient seismic noise ratio is less than a factor of 3. For each frequency (f), if the condition $A_{ij}(f) \geq 3.0 \times B_{ij}(f)$ is satisfied, the seismogram is selected, or otherwise rejected for further analysis. This approach will reduce the effects of ambient seismic noise while at the same time avoiding the degree of arbitrariness present in the scheme. From the selected data set we next compute,

$$O_{ij}(f) = A_{ij}(f) - B_{ij}(f) \ . \tag{3}$$

The smoothing window about each central frequency 1, 3, 5, 7 and 9 Hz is the same for all the cases.

The spectrum of the horizontal motion H is computed from the vector composition of the two horizontal components NS and EW.

The HVSR at the i-th site for the j-th event at each frequency f is then computed as,

$$\mathrm{HVSR}_{ij}(f) = \frac{H_{ij}(f)}{V_{ij}(f)} \ . \tag{4}$$

The event average spectral ratio for each frequency (f) at each i site is finally calculated using 15 events' data and smoothed using a spline interpolator at 0.1 Hz interval from 1 to 10 Hz. The standard deviation of $\mathrm{HVSR}_i^{\mathrm{av}}(f)$ which represents the scatter of individual spectral ratios and hence the statistical uncertainty of the estimated site response values is calculated from

$${}_{\mathrm{std}}\sigma_i = \left\{ \frac{1}{J-1} \sum_{j=1}^{J} \left[\mathrm{HVSR}_{ij} - \mathrm{HVSR}_i^{\mathrm{av}} \right]^2 \right\}^{0.5} \ . \tag{5}$$

►

Figure 5

(a) (i) Unfiltered vertical component (component 1) data recorded at site 7360 for the event 237 of magnitude $M_L = 4.3$. (ii) Butterworth bandpass 0.5–16 Hz filtered vertical component data at site 7360 for the event 237. (iii) Fourier spectrum of the *S*-wave window segment bandpass–filtered Vertical component data. (iv) Fourier spectrum of the background window for the vertical component data. (b) Same as (a), but for NS horizontal component (component 2). (c) Same as (a), but for EW horizontal component (component 3).

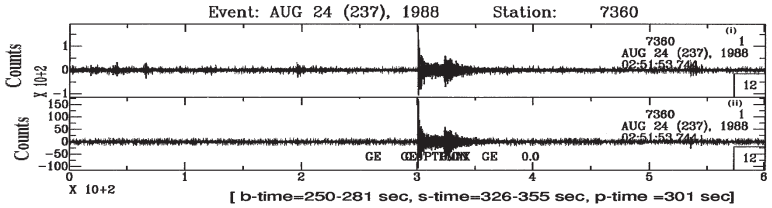
Event: AUG 24 (237), 1988 Station: 7360
Counts
X 10+2
7360 1
AUG 24 (237), 1988
02:51:53.744
[b-time=250-281 sec, s-time=326-355 sec, p-time =301 sec]

(a)

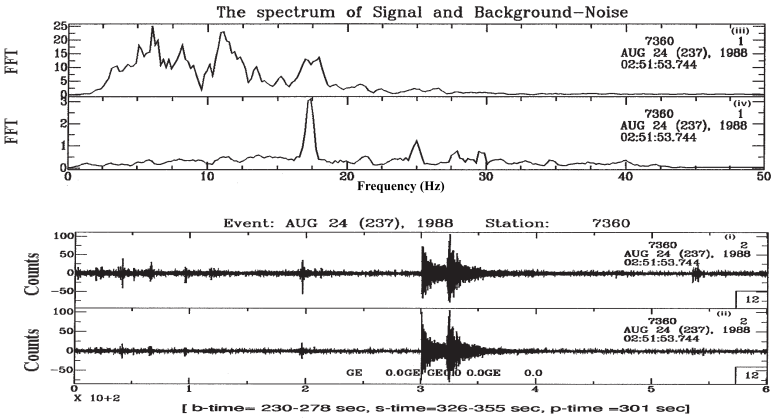
The spectrum of Signal and Background−Noise
FFT
Frequency (Hz)
Event: AUG 24 (237), 1988 Station: 7360
Counts
X 10+2
7360 2
AUG 24 (237), 1988
02:51:53.744
[b-time= 230-278 sec, s-time=326-355 sec, p-time =301 sec]

(b)

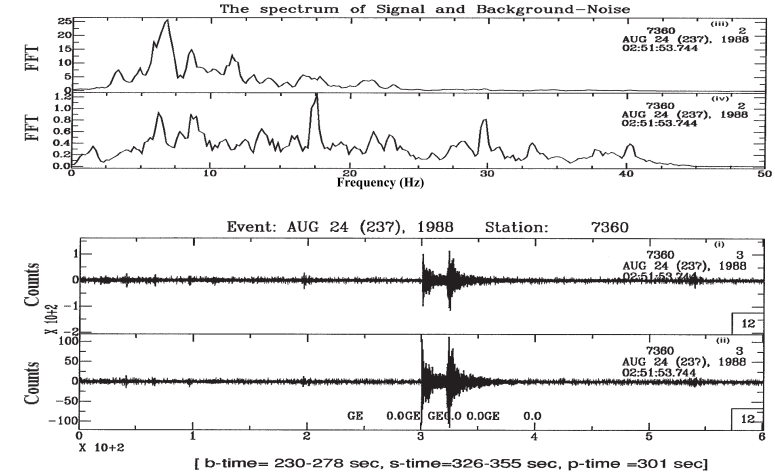
The spectrum of Signal and Background−Noise
FFT
Frequency (Hz)
Event: AUG 24 (237), 1988 Station: 7360
Counts
X 10+2
7360 3
AUG 24 (237), 1988
02:51:53.744
[b-time= 230-278 sec, s-time=326-355 sec, p-time =301 sec]

(c)

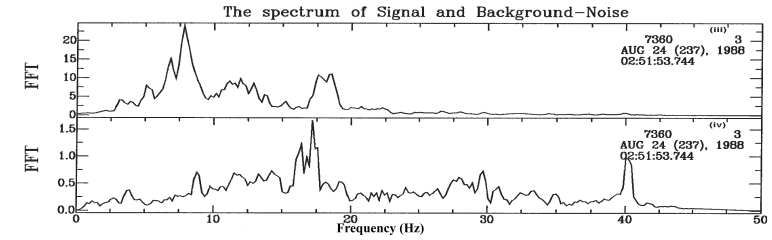
The spectrum of Signal and Background−Noise
FFT
Frequency (Hz)
7360 3
AUG 24 (237), 1988
02:51:53.744

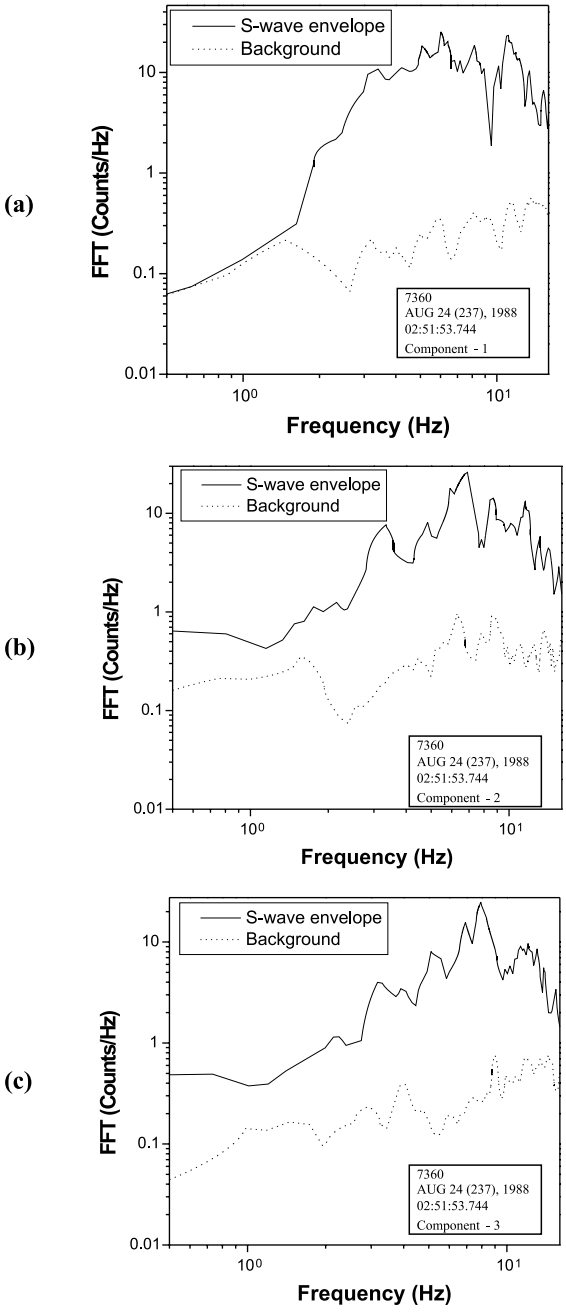

Figure 6
Fourier spectrum of the S-wave and background windows at site 7360 for the event 237 in log-log scale for: (a) Vertical component, (b) NS component and (c) EW component.

The HVSR estimates at frequencies 1–10 Hz at all the stations are presented in Figures 7, 8, 9 and 10. The shaded area (except for stations 7090 and 7365 which recorded one event each) in the diagrams represents $\pm 1_{\text{std}}\sigma_i$ of the central value (the central fine line) obtained at each site. In order to ascertain any scattering effect, a comparison of the radial/vertical versus transverse/vertical spectral ratios is done in log-log scale as shown in Figure 11. The result shows a close agreement (1:1), thereby suggesting that the computed HVSR does not suffer from scattering effect. A closer look at Figure 4 reveals that the events used in the present study are aligned mainly along two azimuthal angles, approximately 225°N and 350°N. We calculated event average HVSR at sites 7063 and 7360 by splitting the events along these source azimuths. The resulting smoothed site response curves at these stations are presented in Figure 12. It is to be noted that along 225°N four events were recorded at 7063 and six at 7360, while along 350°N seven events were recorded at 7063 and eight at

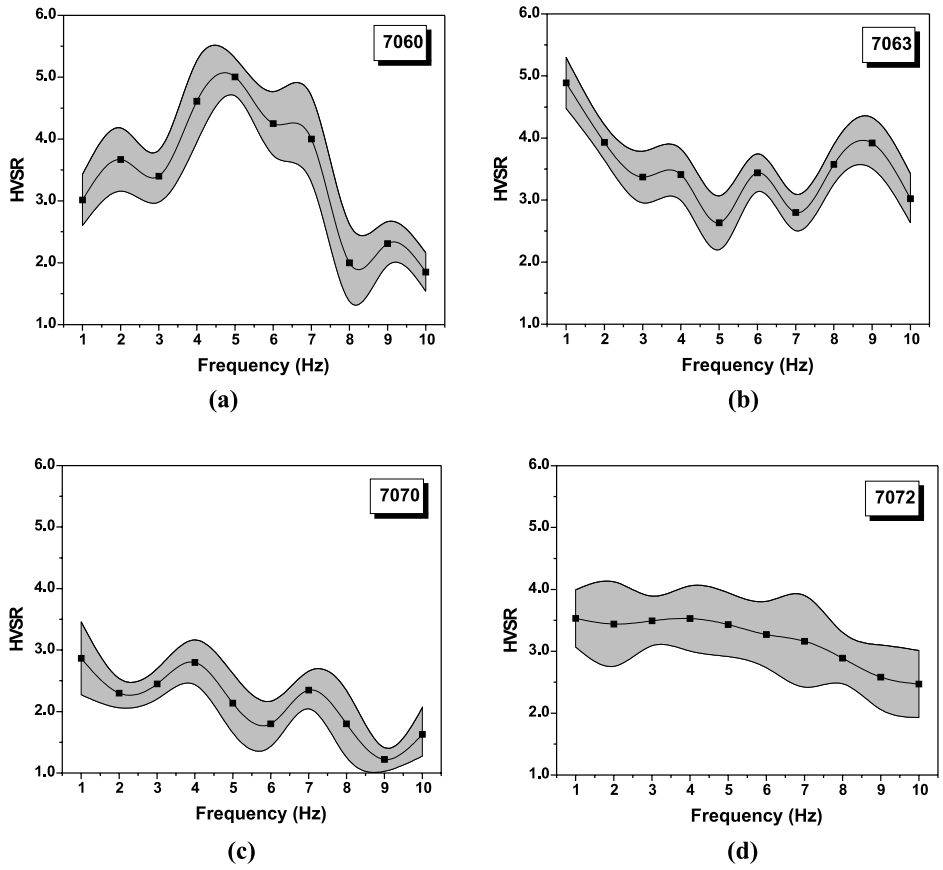

Figure 7
HVSR estimates in 1–10 Hz frequency band at stations. (a) 7060, (b) 7063, (c) 7070 and (d) 7072. The shaded area indicates the uncertainty in ±1 standard deviation of the central value.

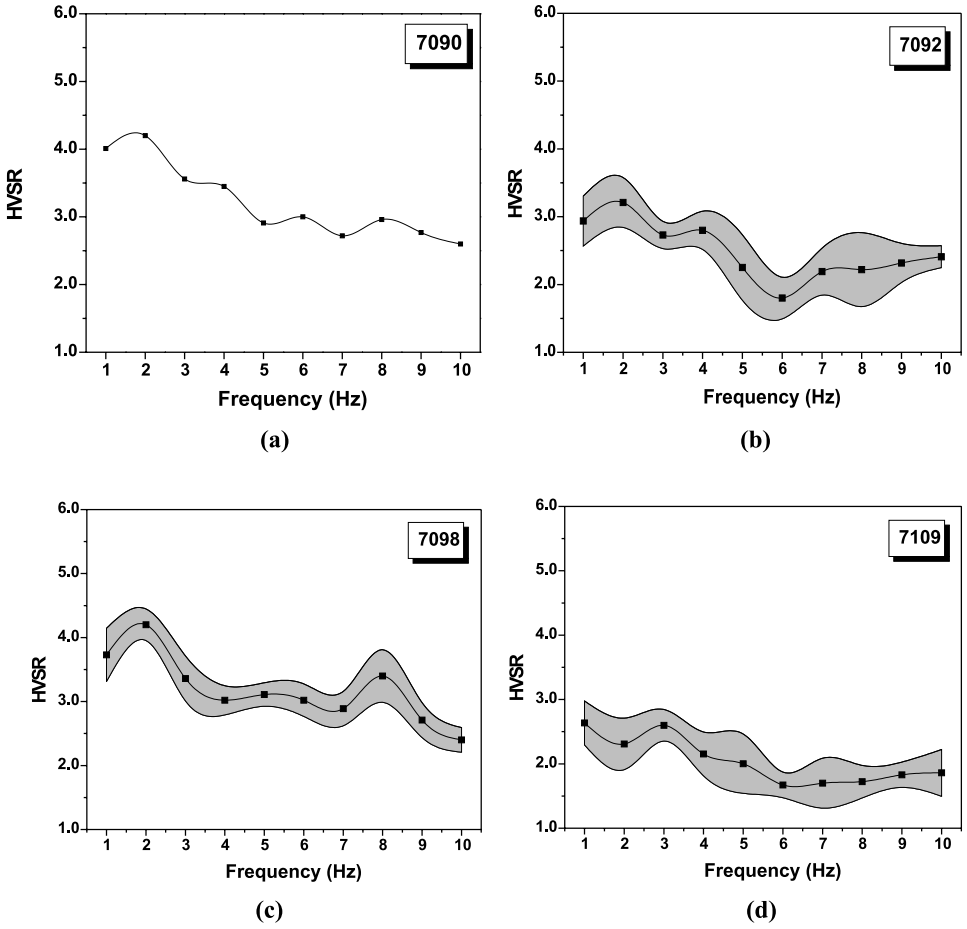

Figure 8
HVSR estimates in 1–10 Hz frequency band at stations. (a) 7090, (b) 7092, (c) 7098 and (d) 7109. The shaded area indicates the uncertainty in ±1 standard deviation of the central value.

7360. The HVSR curves (Figs. 12a and b) along these source azimuths at both the sites are in good agreement. We finally contoured the HVSR site response in the 1–9 Hz frequency band. Here we have presented the results of frequency 1, 5 and 9 Hz in the form of contour maps on the surficial geological map of Greater Anchorage. The respective diagrams are shown in Figures 13, 14 and 15, respectively.

4. Results and Discussion

At 1 Hz (Fig. 13) the HVSR value increases from 2 to 6 from the east (older glacial deposits) to the west (Earthquake Park, Fig. 1) adjoining Knik Arm. The

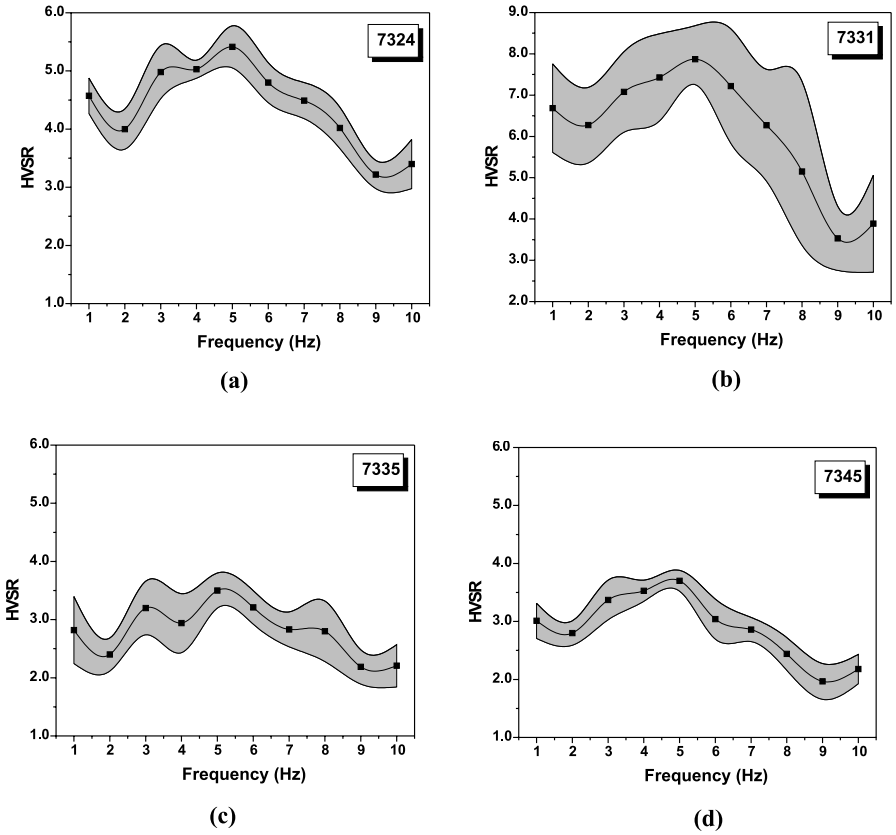

Figure 9
HVSR estimates in 1–10 Hz frequency band at stations. (a) 7324, (b) 7331, (c) 7335 and (d) 7345. The shaded area indicates the uncertainty in ±1 standard deviation of the central value.

areas around Government Hill and the southwestern section of the Elmendorf Air Force Base are associated with HVSR value of 5. However, most parts of the area underlain by the Bootlegger Cove formation are characterized with site response values varying from 3 (south Anchorage) to 5 to 6 in south-central Anchorage, downtown, Woodland Park, Westchester Lagoon (Fig. 1), including Earthquake Park as mentioned earlier.

At 5 Hz (Fig. 14) the spatial distribution of HVSR observed at 1 Hz more or less repeats. The values vary from 2 (older glacial deposits) to 7 in and around Earthquake Park (Fig. 1). At 9 Hz (Fig. 15), the pattern changes from that observed at 1 and 5 Hz, and HVSR values vary from 1 to 4, with the higher value of 4 being associated with the Government Hill area. Note that the contour of this area has been poorly resolved. The central part of the area underlain by the Bootlegger Cove formation has HVSR value of 3.

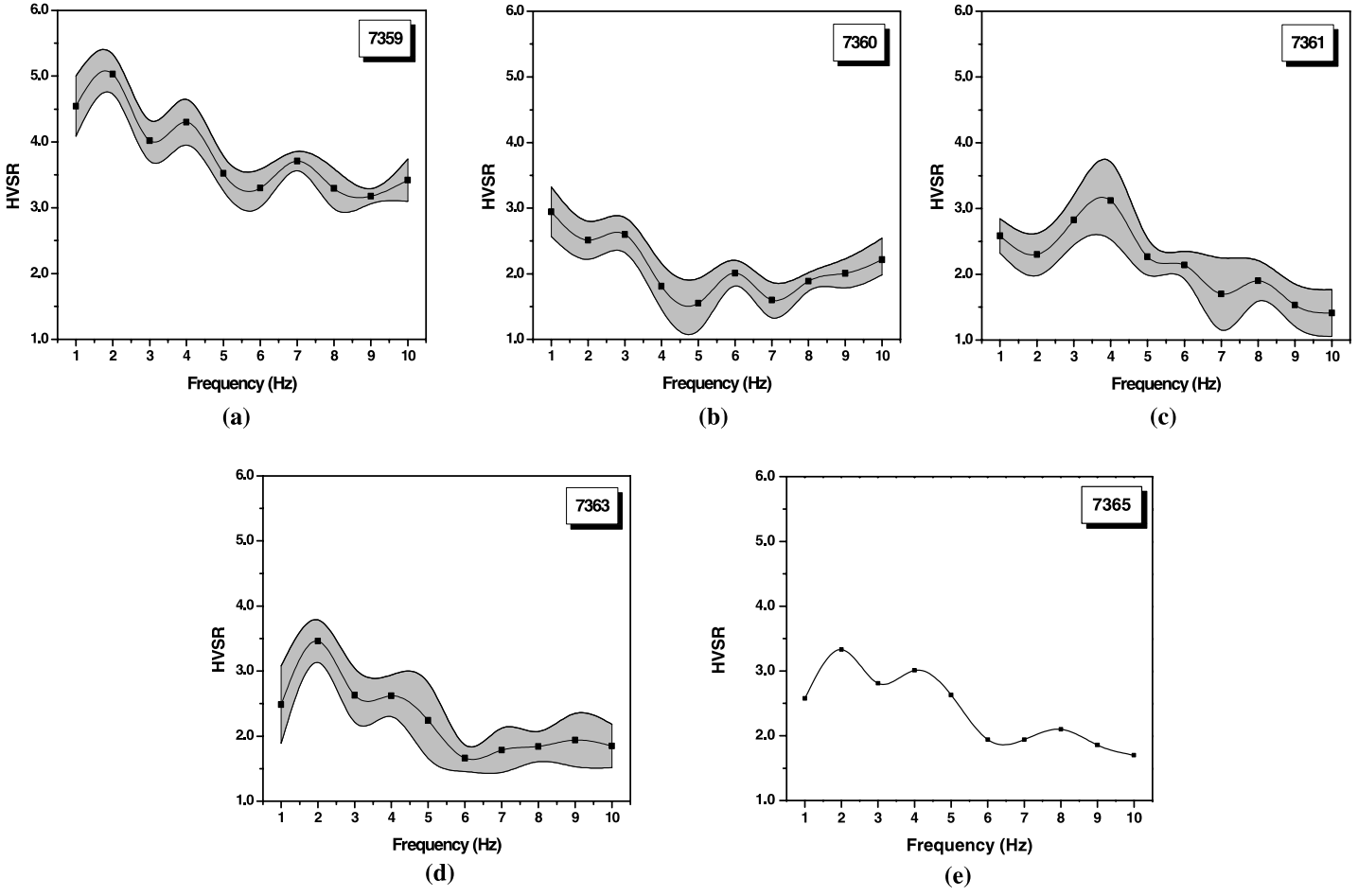

Figure 10
HVSR estimates in 1–10 Hz frequency band at stations. (a) 7359, (b) 7360, (c) 7361, (d) 7363 and (e) 7365. The shaded area indicates the uncertainty in ±1 standard deviation of the central value.

It is necessary to study the influence of the local geology on the spatial variation of site response at different frequencies. On the other hand, the geological information as a function of depth available at this stage for Anchorage is insufficient to achieve the above goal. Nevertheless, in order to overcome the current difficulties we conducted a shear-wave velocity (β) survey at 36 sites in Anchorage in collaboration with the Vibration Instrument Company of Tokyo, Japan and Ensol Corporation of Rayleigh, North Carolina, U.S.A. The field measurements consisted of the determination of short-period (T) phase velocity $C(T)$ for the fundamental mode of Rayleigh waves. The $C(T)$ values were next inverted in terms of β at different depths. The details of the method for 7 calibration sites and all 36 sites mentioned above are given in NATH *et al.* (1997) and DUTTA *et al.* (2000) and not repeated here.

The National Earthquake Hazard Reduction Program (NEHRP) of the United States recommended soil classification based on the average β value in the upper 30 m (CROUSE and MCGUIRE, 1996). In our study, we could obtain β-structure up to 30 m with good resolution (DUTTA *et al.*, 2000). Accordingly, the mean value of β in the 0–30 m depth at each of the 36 sites in Anchorage was computed. The results on soil class based on β distribution following the NEHRP provision are superposed (Fig. 16) on the ground failure susceptibility map of Anchorage which has been prepared by WINTERHALDER *et al.* (1979).

The seismic-related ground failure susceptibility has been rated to one to five scales from low susceptibility to high. The specific criteria for each rating are

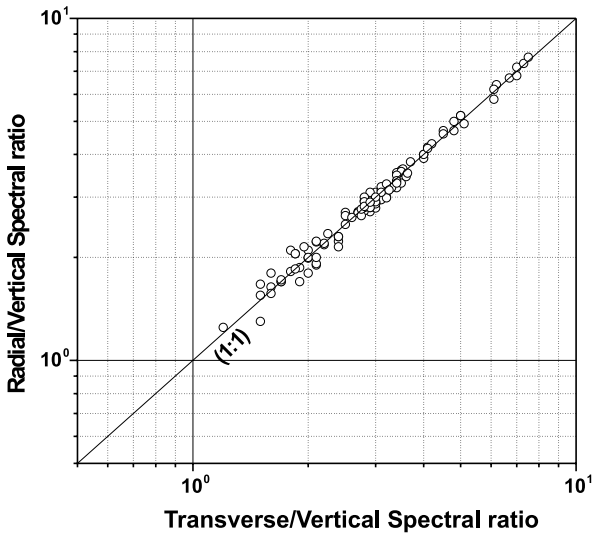

Figure 11
The comparison of the Radial/Vertical versus Transverse/Vertical spectral ratio estimates. The solid diagonal line indicates 1:1 correspondence.

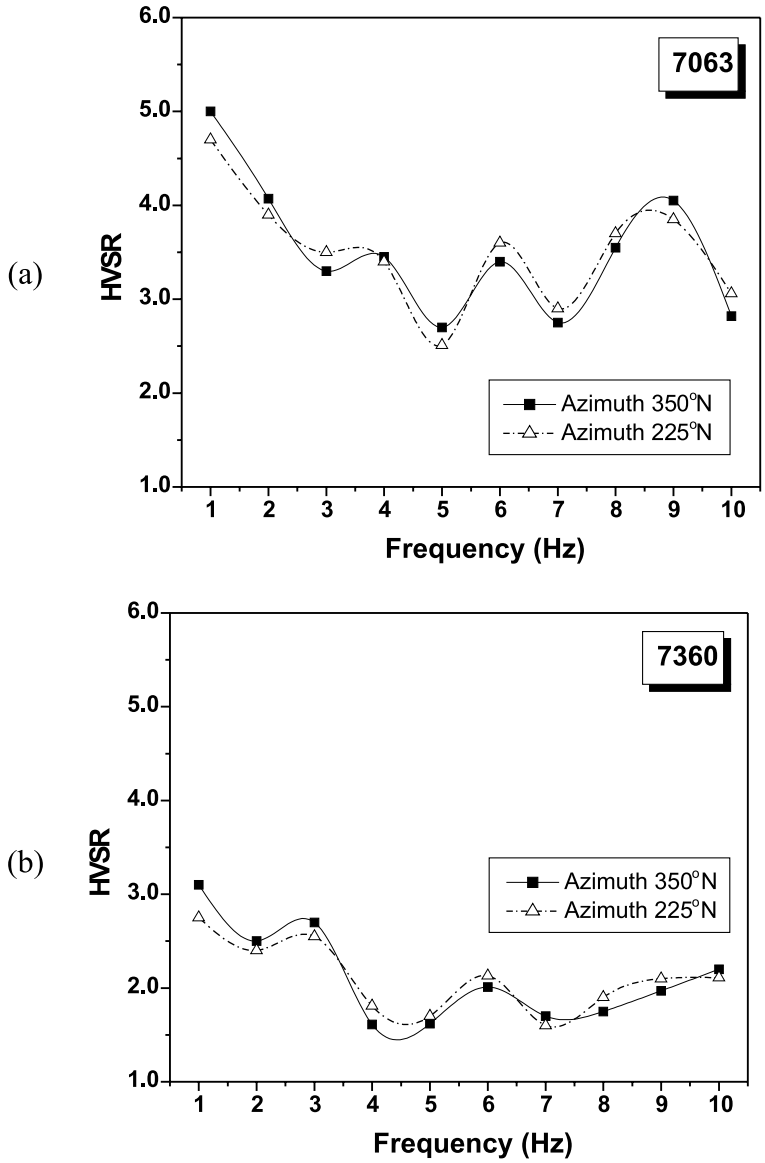

Figure 12
The comparison of HVSR estimates in the 1–10 Hz frequency band by splitting the recorded events into two groups of source azimuths 225°N and 350°N (approximately). The analysis is performed at sites: (a) 7063 and (b) 7360.

described in the map legend given in Fig. 16 (WINTERHALDER *et al.*, 1979). These criteria were developed by consideration of the observed and expected seismic response of various combinations of soil, geologic and topographic conditions

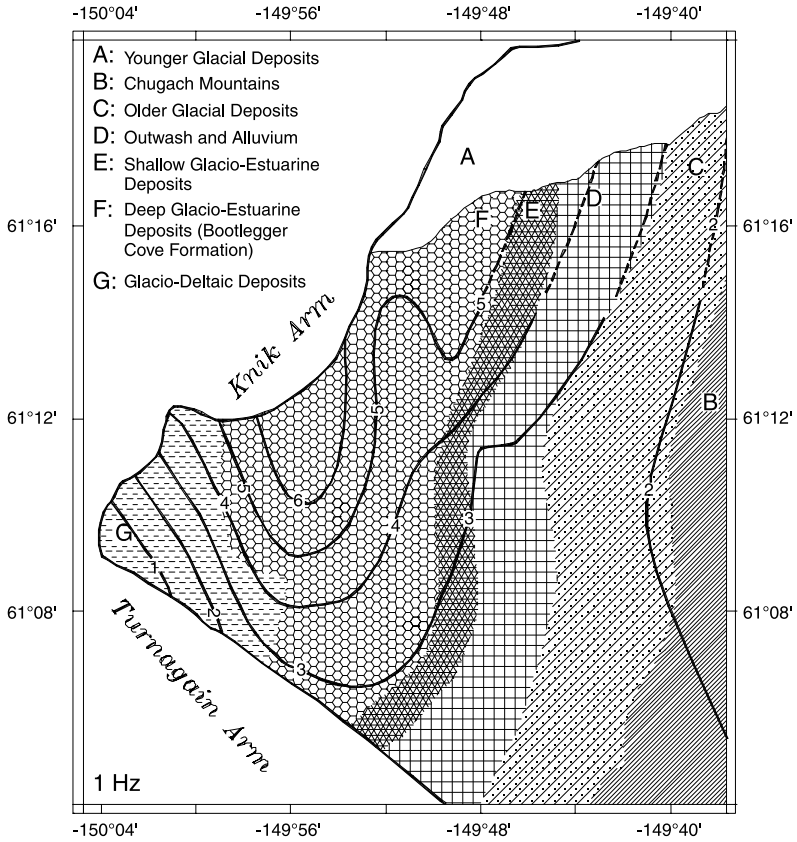

Figure 13
Spatial distribution of HVSR value obtained at 1 Hz shown on the surficial geology map of Anchorage.

(based on observations in Anchorage as well as observations and research in areas which have conditions similar to those at Anchorage) (SHANON and WILSON, 1964). In general, the susceptibility is least in areas of exposed bedrock; moderate in areas underlain by dense, coarse-grained, unconsolidated sediments (such as glacial till); and greatest in areas which are underlain by saturated, fine-grained, unconsolidated deposits. Surficial geologic and interpretive maps provided the basis for susceptibility rating. The lowest ground failure susceptibility is observed in the rock sites of Chugach Mountain geological province (Fig. 1). Moderately low ground failure is rated for younger glacial deposits, transition zone and part of the marginal zone *D*. Moderate ground failure susceptibility is rated for Bootlegger Cove Clay, part of the western fringe of marginal zone *G* and scattered thin lenses elsewhere. High susceptibility is found along the coastal fringes and very high along Knik Arm, coinciding with the area of extensive landslides following the

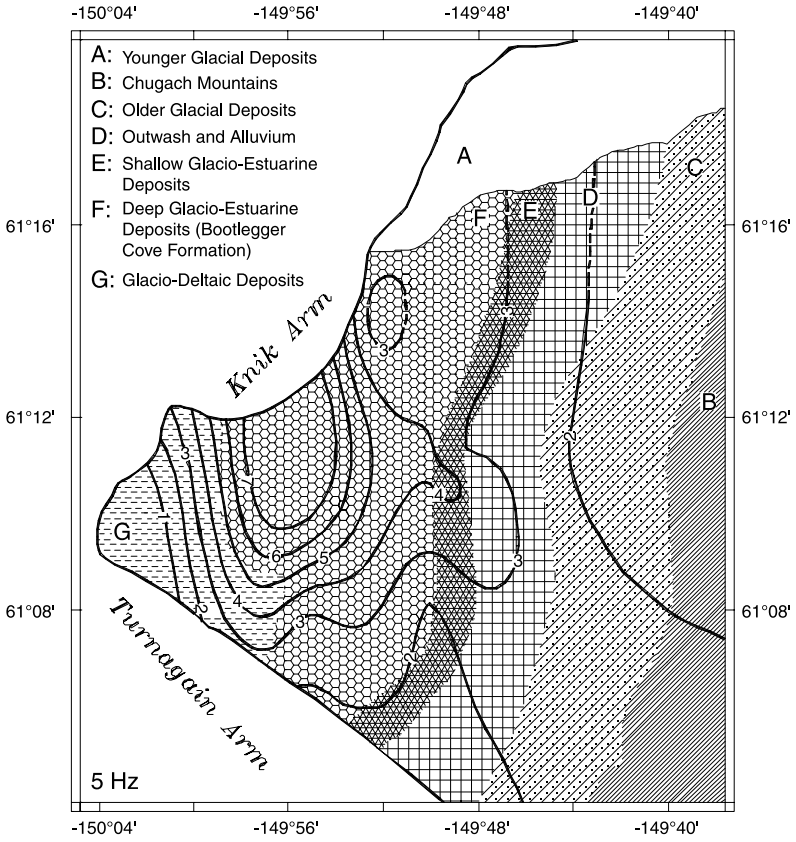

Figure 14
Spatial distribution of HVSR obtained at 5 Hz shown on the surficial geology map of Anchorage.

1964 earthquake. Turnagain Height Arm is characterized mostly by coastal mud flats. Some localized areas contain conditions which could be susceptible to seismically induced ground failure but were not included in this generalized map of Figure 16.

The results in Figure 16 show that the soil class degrades from B ($\beta > 760$ m/s) in the eastern side to D (180 m/s $< \beta \leq 360$ m/s) in the west and further degrades to class *E* ($\beta \leq 180$ m/s) (not constrained well) in the Government Hill area and southern part of the Elmendorf Air Force Base. However, a large part of the area underlain by Bootlegger Cove formation belongs to soil class *C* (360 m/s $< \beta \leq 760$ m/s). In south Anchorage, a small area with soil class *D* occurs adjoining Turnagain Arm.

The HVSR distribution at 1 and 5 Hz (Figs. 13 and 14) shows close similarity with the spatial variation of soil class, with the exception of the area in and around Kincaid Park (Fig. 1). Here both at 1 and 5 Hz, we obtained HVSR

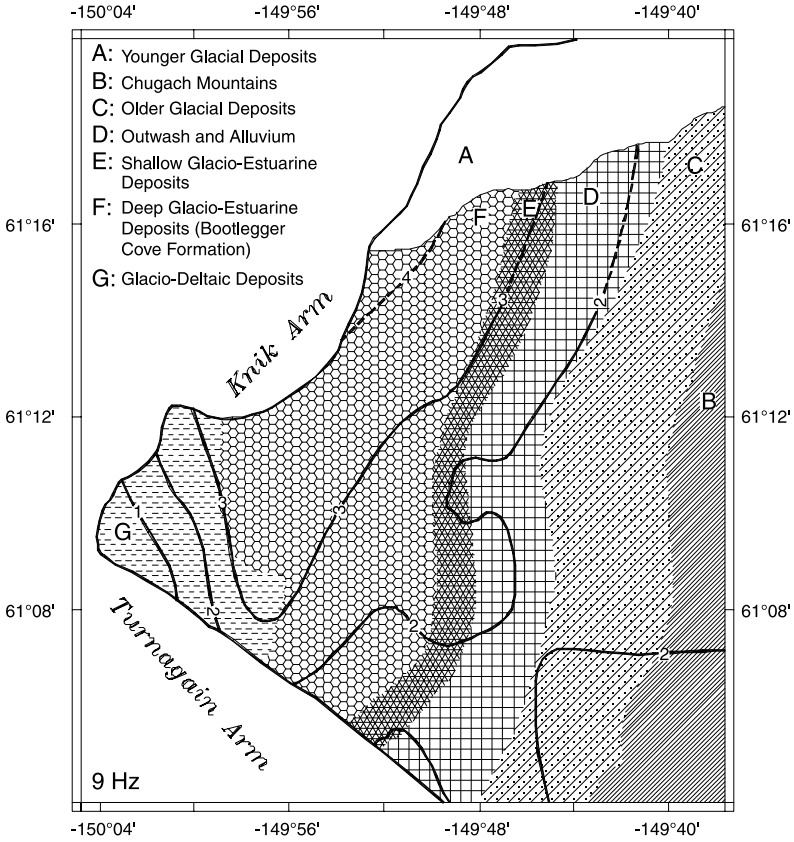

Figure 15
Spatial distribution of HVSR obtained at 9 Hz shown on the surficial geology map of Anchorage.

values comparable to those associated with the foothill area of Chugach Mountains on the east. On the other hand, the soil class tends to be of the same class as obtained for the high site response area, like the Earthquake Park area. Similarly, the small area of soil class *D* in south Anchorage has no counterpart seen in HVSR distribution. However, the areas of high HVSR, particularly along Knik Arm, manifest good agreement with areas of high ground failure susceptibility (Fig. 16).

In order to compare HVSR values obtained from the weak motion data with that expected from strong motion data, we installed a network of 22 strong motion stations in the Anchorage area. The stations are equipped with Kinematrics Altus K2 sensors with trigger level set at 0.05 percent of the full scale of 2 g. The results of the analysis of the data currently being recorded by this network will be reported in the future.

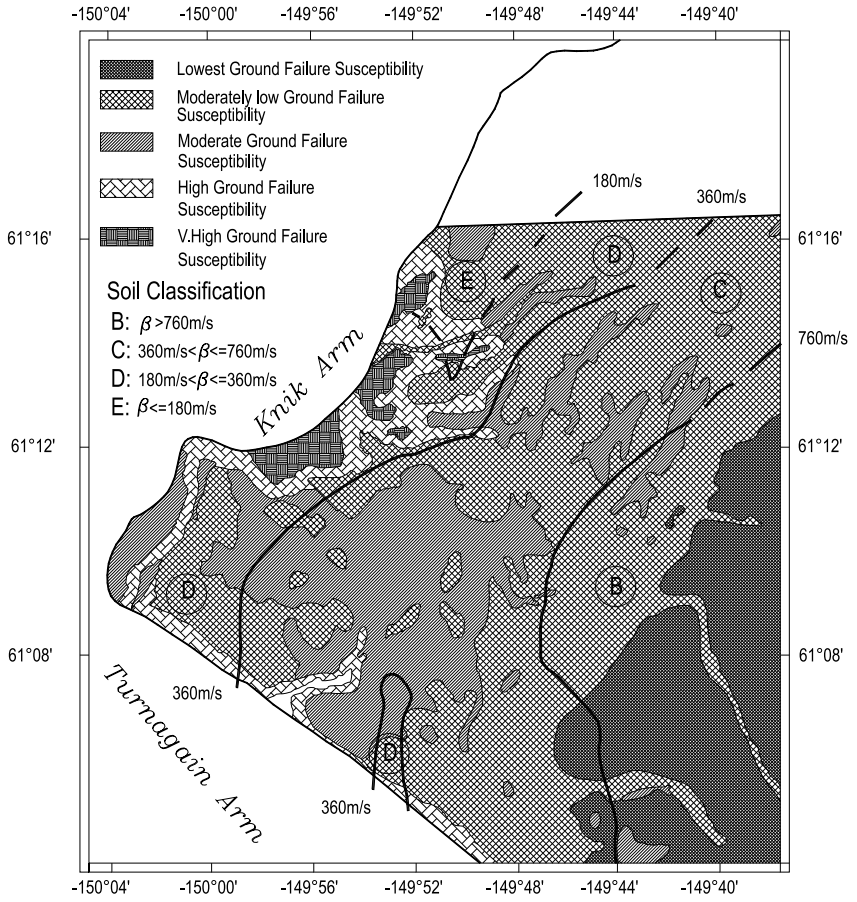

Figure 16
Solid and broken (poorly constrained) contour lines represent the boundary of the transition from one class of soil to the next. The background map shows the ground failure susceptibility in Anchorage prepared by WINTERHALDER *et al.* (1979).

Acknowledgements

The authors are grateful to Artak Martirosyan and Utpal Dutta for many valuable discussions and Mitch Robinson, all of the Geophysical Institute, University of Alaska Fairbanks in assisting with computer hardware. We thank the referee Enrico Priolo for his critical review and helpful comments which greatly improved the quality of the paper. Special thanks are due to Fabio Romanelli for his efficient handling of the manuscript. The first author (SKN) gratefully acknowledges the financial and research support provided to him by the Geophysical Institute, University of Alaska Fairbanks, U.S.A. during his sabbatical tenure as Visiting

Scientist at GI during 1995–96. This research was supported in part by Alaska Science and Technology Foundation Grant No. 91–2–125.

References

AKI, K. (1988), *Local Site Effects on Strong Ground Motion*, Proc. of Earthq. Eng. and Soil Dynamics *II*, 103–155.

AKI, K. and IRIKURA, I. (1991), *Characterization and Mapping of Earthquake Shaking for Seismic Zonation*, Proc. 4th Int. Conf. Seismic Zonation 1, Stanford, California, 61–110.

AMMON, C. J. and ZANDT, G. (1993), *Receiver Structure beneath the Southern Mojave, California*, Bull. Seismol. Soc. Am. *83*, 737–755.

ANDREWS, D. J. *Objective determination of source parameters and similarity of earthquakes of different size*. In *Earthquake Source Mechanics* (eds. Das S., Boatwright, J., and Scholz, C. H.) (American Geophysical Union, Washington D.C.(1986)), pp. 259–268.

BARD, P. Y. (1994), *Effects of Surface Geology on Ground Motion: Recent Results and Remaining Issues*, Proc. 10th European Conf. on Earthq. Eng., Vienna, *1*, 305–325.

BOATWRIGHT, J., SEEKINS, L. C., and MUELLER, C. S. (1991), *Ground Motion Amplification in the Marina*, Bull. Seismol. Soc. Am. *81*, 1980–1997.

BORCHERDT, R. D. (1970), *Effects of Local Geology on Ground Motion near San Francisco Bay*, Bull. Seismol. Soc. Am. *60*, 29–61.

CROUSE, C. B. and MCGUIRE, J. W. (1996), *Site Response Studies for Purpose of Revising NEHRP Seismic Provisions*, Earthq. Spectra *12*, 407–439.

DIMITRIU, P. P., PAPAIOANNOU, Ch. A., and THEODULIDIS, N. P. (1998), *Euro-seistest Strong-motion Array near Thessaloniki, Northern Greece: A Study of Site Effects*, Bull. Seismol. Soc. Am. *88*, 862–873.

DUTTA, U., BISWAS, N. N., MARTIROSYAN, A., NATH, S., DRAVINSKI, M., PAPAGEORGIOU, A., and COMBELLICK, R. (2000), *Delineation of Spatial Variation of Shear-wave Velocity with High-frequency Rayleigh Waves in Anchorage, Alaska*, Geophys. J. Int. *147*, 365–375.

FIELD, E. H. and JACOB, K. H. (1995), *A Comparison and Test of Various Site-response Estimation Techniques, Including Three that are not Reference-site Dependent*, Bull. Seismol. Soc. Am. *85*, 1127–1143.

LAHR, J. C., PAGE, R. A., STEPHENS, C. D., and FOGLEMAN, K. A. (1986), *Sutton, Alaska, Earthquake of 1984; Evidence for Activity on the Talkeetna Segment of the Castle Mountain Fault System*, Bull. Seismol. Soc. Am. *76*, 967–983.

LANGSTON, C. A. (1979), *Structure under Mount Rainier, Washington, Inferred from Teleseismic Body Waves*, J. Geophys. Res. *84*, 4749–4762.

LERMO, J. F., FRANCISCO, S., and CHAVEZ-GARCIA, J. (1993), *Site Effect Evaluation Using Spectral Ratios with only One Station*, Bull. Seismol. Soc. Am. *83*, 1574–1594.

NAKAMURA, Y. (1989), *A method for Dynamic Characteristics Estimation of Subsurface Using Microtremor on the Ground Surface,* QR Railway Tech. Res. Inst. *30*, 1.

NATH, S. K., CHATTERJEE, D., BISWAS, N. N., DRAVINSKI, M., COLE, D. A., PAPAGEORGIOU, A., RODRIGUEZ, J. A., and PORAN, C. J. (1997), *Correlation Study of Shear-wave Velocity in Near-surface Geological Formations in Anchorage, Alaska*, Earthq. Spectra *13*, 55–75.

OWENS, T. J. and CROSSEN, R. S. (1988), *Shallow Structure Effects on Broadband Teleseismic P Waveforms*, Bull. Seismol. Soc. Am. *78*, 96–108.

OWENS, T. J., ZANDT, G., and TAYLOR, S. R. (1984), *Seismic Evidence for an Ancient Rift beneath the Cumberland Plateau, Tennessee: A Detailed Analysis of Broadband Teleseismic P Waveforms*, J. Geophys. Res. *89*, 7783–7795.

RATCHKOVSKY, N. A., PUJOL, J., and BISWAS, N. N. (1997), *Relocation of Earthquakes in the Cook Inlet Area, Southcentral Alaska, Using the Joint Hypocenter Determination Method*, Bull. Seismol. Soc. Am. *87*, 620–636.

SHANNON and WILSON (1964), *Report on Anchorage Area, Soil Studies, Alaska*, prepared for US Army. Dist., Anchorage, Alaska, Contract No. DA-95-507-CIVENG-64-18.

TAKAHASHI, K., OHNO, S., TAKEMURA, M., OHTA, T., HATORI, T., and OMOTE, S. (1992), *Observation of Earthquake Strong-motion with Deep Borehole Generation of Vertical Motion Propagating in Surface Layers after S-wave Arrival,* Proc. of the 10th World Conf. of Earthquake Eng. *3*, 1245–1250.

UPDIKE, R. G. and ULERY, C. A. (1983), *Preliminary Geologic Map of the Anchorage B-6 NW (Eklutna Lake) Quadrangle, Alaska*, Alaska Div. of Geological and Geophysical Surveys, Report No. 83–8.

WHITMAN, R. V. (ed.) (1989), Workshop on *Ground Motion Parameters for Seismic Hazard Mapping*, Technical Report NCEER-89-0038.

WINTERHALDER, E. C., WILLIAMS, T. L., and ENGLAND, J. M. (1979), *Geotechnical Hazards Assessment, Municipality of Anchorage, Anchorage, Alaska*, Harding-Lawson Associates.

WOODWARD-CLYDE CONSULTANTS (1982), *Anchorage Office Complex, Geotechnical Investigation*, Report to Alaska Department of Transportation and Public Facility, I-III, Anchorage, Alaska.

YEHLE, L. A., ODOM, J. K., SCHMOLL, H. R., and DEARBORN, L. L. (1986), *Overview of the Geology and Geophysics of the Tikishla Park Drillhole*, USGS A-84-1, Anchorage, Alaska, U.S.G.S., Open-File Report 86–293.

(Received January 18, 2001, accepted July 15, 2001)